Alteration of Pool Boiling Heat Transfer on Metallic Surfaces by In Situ Oxidation

Youngsup Song[1], Hyeongyun Cha[1], Zhen Liu[2], Jee Hyun Seong[3], Lenan Zhang[1], Daniel J. Preston[2], Evelyn N. Wang[1]*

[1]Department of Mechanical Engineering, Massachusetts Institute of Technology, Cambridge, MA 02139, USA

[2]Department of Mechanical Engineering, Rice University, Houston, TX 77005, USA

[3]Department of Nuclear Science and Engineering, Massachusetts Institute of Technology, Cambridge, MA 02139, USA

[*]Author to whom correspondence should be addressed: enwang@mit.edu

KEYWORDS

Critical heat flux, Heat transfer coefficient, Metal oxide nanostructures, Wettability

ABSTRACT

The critical heat flux during pool boiling has been investigated for a range of applications including electrical power generation and thermal management. Reported experimental CHF values during pool boiling of water on flat metallic surfaces, however, show a large discrepancy across studies. Here, we address this discrepancy in CHF values by accounting for oxidation of metallic surfaces during boiling. We studied the effect of in situ oxidation on flat Cu and Ni surfaces by changing the duration that samples were held in saturated water before conducting boiling experiments. The morphology and chemical composition of surfaces after the boiling experiments were analyzed by atomic force microscopy and X-ray photoelectron spectroscopy, respectively. Cu surfaces showed gradually increasing CHF values as the duration in saturated water increased, which could be attributed to the increase in roughness due to the formation of Cu_2O nanostructures. Conversely, Ni surfaces showed relatively stable CHF and morphology as a nearly flat layer of NiO formed, with one exception: formation of a highly wetting hydroxide, $Ni(OH)_2$, on a Ni coupon held in saturated water for 24 h resulted in a uniquely high CHF value, signifying the importance of surface chemistry in addition to morphology. The fundamental mechanisms resulting in the wide spread of CHF values on metallic surfaces elucidated in this work will lead to more accurate estimation of CHF as well as a deeper mechanistic understanding of CHF values on engineered surfaces.

1. Introduction

Boiling is an essential process in many industrial applications, including electrical power generation and high flux thermal management. A boiling performance parameter of particular interest is the critical heat flux (CHF, q''_{CHF}), which represents the operational heat flux limit of nucleate boiling. During nucleate boiling, vapor bubbles nucleate and coalesce with each other before they detach from a boiling surface, but as the applied heat flux reaches the CHF, bubble growth and coalescence events become too rapid for sustained departure, and an insulating vapor layer forms over the surface. The abrupt increase in thermal resistance due to this vapor layer causes thermal runaway and critical failure of the boiling system. While extensive efforts over the past decades have focused on engineering boiling surfaces to achieve CHF enhancement compared to that of a pristine and flat surface [1], CHF values of flat surfaces for pool boiling of water show a large discrepancy across the literature, even for the same material (Figure 1). Note that the literature data included in Figure 1 are based on horizontal and upward-facing heaters in saturated water at the atmospheric pressure. For example, CHF values on flat silicon (Si) and silicon dioxide (SiO_2) vary across the literature roughly from 60 to 110 W/cm^2. Metallic surfaces such as copper (Cu) and nickel (Ni) show even wider spreads in CHF values, exceeding Zuber's CHF prediction for a flat surface [2]. Understanding the cause of this discrepancy is important for two reasons. First, an inaccurate CHF estimation could be detrimental for boiling applications such as nuclear power plants, where safety is the foremost concern. Second, the flat surface CHF is particularly important for a mechanistic understanding of CHF because the flat surface CHF is used as a baseline value to which the enhancement of engineered surfaces is compared. Previously, the spread in CHF values of flat SiO_2 surfaces was addressed by accounting for

airborne hydrocarbon adsorption [3]. Experimental results of CHF values and the amount of adsorbed hydrocarbons on flat SiO_2 surfaces showed that the hydrocarbon adsorption on boiling surfaces could lower the CHF values by decreasing the surface wettability.

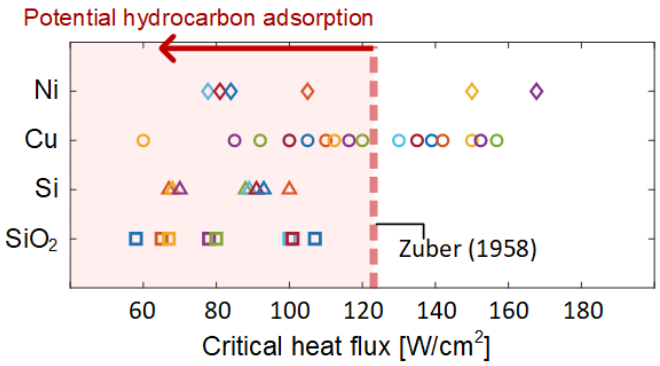

Figure 1. Large spread in reported CHF values during saturated pool boiling of water at atmospheric pressure on smooth, horizontal, and upward-facing nickel [4-9], copper [10-23], silicon [24-31], and silicon dioxide surfaces [32-42]. Compared to Si and SiO_2, CHF values of flat Cu and Ni surfaces show larger discrepancies across studies, where some results show even higher CHF values compared to the Zuber's CHF estimation for a flat surface. All data used in this plot are summarized in the Supporting Information Table S1.

However, the larger spread in CHF values of metallic surfaces, where some results show even higher values than Zuber's CHF prediction (125 W/cm^2 for water), cannot be explained by hydrocarbon adsorption. This is because Zuber's prediction is slightly higher than the CHF value of a smooth and clean surface [3], while hydrocarbon adsorption only lowers CHF values. The different methods of heat flux characterization and experimental measurement uncertainty could

contribute up to ~20% CHF uncertainty [43]; yet, literature CHF values reported for Cu and Ni vary by a much larger range, up to 157 and 168 W/cm^2, respectively. Note that CHF values can also vary with a heater size according to hydrodynamic instability-based explanations [44, 45]. Empirical literature data, however, have shown controversial results for the effects of heater size [44-46], which may be attributed to experimental error or to a phenomenon that has not yet been identified. In this work, we address one possible mechanism of the unexplained elevated CHF on metals by accounting for oxidation of metallic surfaces during boiling by testing Cu and Ni surfaces. Thermodynamically, both Cu and Ni are stable in pure, oxygen-free water; for example, the chemical stability of Cu in 400 ℃ water has been experimentally demonstrated [47]. Nonetheless, the oxidation, i.e., corrosion, of Cu and Ni in water has been reported because, in practice, metals can react with dissolved oxygen in water and outgassing hydrogen from the metal samples themselves or from the experimental apparatus [48-50]. In particular, Saadi et al. tested the corrosion of various metals in water at 75 and 95 ℃; they found that a wide range of metals including Cu and Ni can corrode and form metal oxide nanostructures in hot water [48]. Because nanostructures on a boiling surface can increase CHF during pool boiling [5, 6, 13, 25, 27-30], the oxidation of metals and resulting formation of metal oxide nanostructures should be a key contributing factor in the spread in reported CHF values depending on the degree of oxidation.

2. Experimental

2.1 Sample preparation

To investigate the oxidation of metallic surfaces during boiling and its effects on pool boiling heat transfer, we held Cu and Ni samples in saturated water for different periods of time (30 min, 7 h, and 24 h) before conducting pool boiling experiments. We prepared two different types of Cu and Ni samples that are commonly used for boiling research: (i) thin metal films coated on silicon wafers and (ii) bulk metal coupons. The thin-film samples were prepared by sputtering a 10 nm Ti adhesion layer followed by a 100 nm Cu or Ni layer on diced 650-μm-thick silicon chips (20×20 mm^2) covered with thermally grown 1 μm SiO_2 layers. Cu and Ni coupons were prepared by cutting metal sheets (813 μm-thick 110 copper and 483 μm-thick 200 nickel, McMaster-CARR) into 15×15 mm^2 squares with a waterjet. Metal coupons were smoothed with sandpaper (CarbiMet, Buehler) of up to 800 grit and subsequently polished with diamond suspensions of 1 and 3 μm (MetaDi Polycrystalline Diamont Suspensions, Buehler) to make the surface flat at the microscale. For convenience, we refer to each sample based on its duration in saturated water before boiling, material, and surface type; for example, a “24 h Ni thin film” means a Ni thin film surface left in saturated water for 24 h before boiling. Prior to boiling, all samples were cleaned in 2.0 M hydrochloric acid solution for 10 minutes to remove the native oxide and any organic contaminants.

2.2 Pool boiling experiment

We used two different pool boiling setups for the sputtered thin film samples and the metal coupons. For thin film samples, we created a 100 nm serpentine platinum (Pt) heater defining the heating area A_h of 10 × 10 mm^2 on the backside of each sample, through which heating power was applied. The applied heat flux (q''_{in}) was characterized by measuring the voltage drop (V) and current (I) across the heater, i.e., q } rsub {in} =IV/ {A} rsub {h¿. The serpentine Pt heater also served as a resistive temperature detector for temperature characterization.

In the case of metal coupons, we soldered the samples to a copper block using solder paste. The copper block has the same cross-sectional area (15 × 15 mm^2) as the samples, which defines the heating area. At the center axis of the copper block, three K-type thermocouples were inserted with a 5 mm spacing (Δx). The bottom of the sample-mounted copper block was then attached to another copper block in which five 250 W cartridge heaters were embedded to provide power for the boiling heat flux. The heat flux (q'') was characterized from the temperature gradient of the three thermocouples using Fourier's law with a three-point backward finite difference approximation, i.e.,

q = {k} rsub {Cu} {left (3 {T} rsub {1} -4 {T} rsub {2} + {T} rsub {3} right)} / {left (2 Δ x right)

, where T_1, T_2, and T_3 are the temperature measurements from the top, middle, and bottom thermocouples, respectively, from the sample. Here k_{Cu} is the temperature-dependent thermal conductivity of copper ($k_{Cu} = 2.83 \times 10^4 T^2 - 0.165 T + 378.1$ [W/m-K], where temperature T is in Kelvin) [43]. An additional thermocouple inserted beneath the sample was then used to calculate the wall superheat combined with the measured heat flux. Each boiling experiment took ≈ 30

minutes on average. Further details of pool boiling experiments and measurement uncertainty are available in Section II of the Supporting Information.

3. Results and discussion

3.1 Pool boiling results

Figure 2 shows the pool boiling curves, i.e., heat flux (q'') as a function of wall superheat (ΔT_w), of Cu and Ni samples. Here ΔT_w is the temperature difference between the boiling surface and the saturated liquid. Both Cu thin films and Cu coupons showed apparent changes in pool boiling heat transfer associated with the duration (Δt) left in saturated water before boiling (Figure 2a, b). As Δt increased from 30 min to 24 h, pool boiling curves shifted upward to the left monotonically, representing increasing CHF and heat transfer coefficient (HTC). Here HTC is the slope of a boiling curve from the origin by definition, i.e., $HTC = q/\Delta$ {T} rsub {w. The boiling curves of the Cu thin film samples (Figure 2a) showed more significant changes than the coupons. For example, CHF values of Cu thin films were 96.8, 120.9, and 133.7 W/cm^2 for Δt of 30 min, 7 h, and 24 h, respectively, which increased 38% from Δt of 30 min to 24 h. In addition, HTC values at CHF of Cu thin films increased from 24.5 to 54.4 kW/m^{2}K from Δt of 30 min to 24 h, a 122% increase in HTC. While less significant compared to Cu thin films, Cu coupons (Figure 2b) also showed increases in CHF and HTC at CHF values by 17.6 and 44%, respectively, as Δt increased from 30 min to 24 h.

Conversely, Ni surfaces exhibited relatively stable boiling heat transfer compared to Cu surfaces. CHF values of Ni thin films changed marginally, e.g., 99.0, 99.1, and 106.8 W/cm^2 for

Δt of 30 min, 7 h, and 24 h, respectively. Changes in HTC values were also insignificant, which showed HTC at CHF values of 27.7, 22.0, and 27.1 kW/m^{2}K for 30 min, 7 h and 24 h, respectively. 30 min and 7 h Ni coupons followed the stable trend, where CHF values were 88.5 and 92.5 W/cm^2, respectively. The 24 h Ni coupon, however, showed a noticeably higher CHF value of 121.3 W/cm^2 (we discuss the mechanism for this increase in Section 3.3).

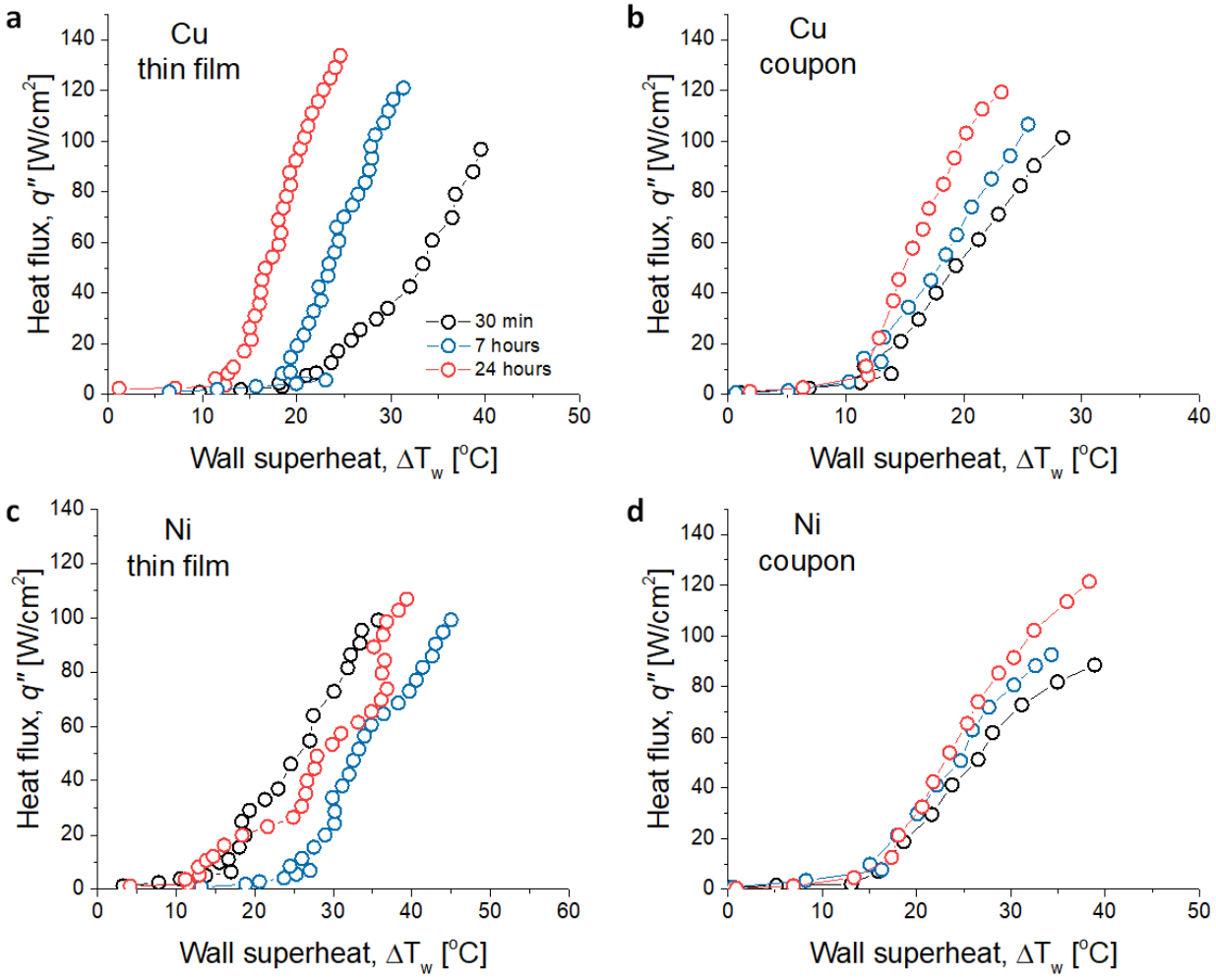

Figure 2. Pool boiling curves of (a) Cu thin film, (b) Cu coupon, (c) Ni thin film, and (d) Ni coupon surfaces. The surfaces were left in saturated water for different periods of time (30

minutes (black), 7 hours (blue), and 24 hours (red)) before measurements. The experimental uncertainty is smaller than the marker size in the plots.

In addition to boiling curves, we plotted CHF values ($q"_{CHF}$) normalized by the CHF of a corresponding material and type with 30 min Δt ($q"_{CHF,30min}$) as a function of Δt to investigate the relative change in CHF values (Figure 3). Along with Ni and Cu, we also plotted the results of chemically stable SiO_2 surfaces for reference. The plot shows clear increasing trends of CHF values of Cu surfaces as Δt increased. CHF values of Ni thin films were as stable as those of SiO_2 reference surfaces, while the Ni coupon with 24 h Δt showed the relative change in CHF value as significant as Cu thin films.

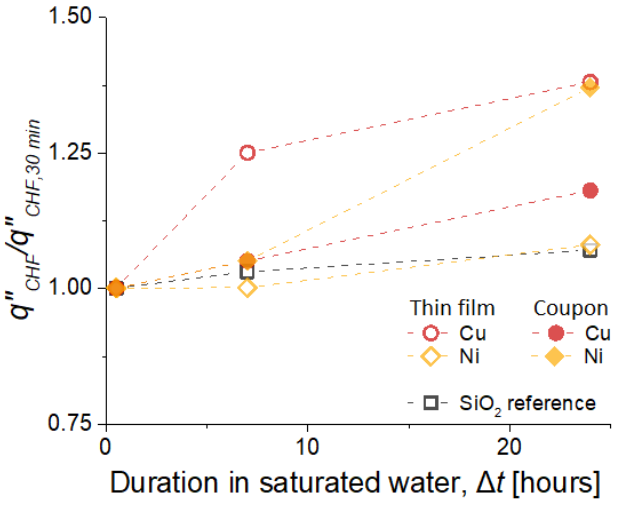

Figure 3. Relative change in CHF values as the duration in saturated water before boiling increases.

3.2 Change in morphology

The changes in CHF values shown in Section 3.1 indicate that surface material and structural properties were altered in a favorable way for pool boiling heat transfer as Δt increases. In this section, we investigate the change in surface morphology using scanning electron microscopy (SEM) and atomic force microscopy (AFM). Figure 4 shows the SEM images of Cu and Ni surfaces before being immersed in saturated water and after boiling with different Δt. SEM images of surfaces before being immersed in saturated water show the initial surface conditions, where thin film surfaces represent fine grains resulting from sputtering and coupons show sandpaper scratches. Although the kinetics of nanostructure growth seems different for thin films and coupons, the SEM images of Cu surfaces show growing nanostructures as Δt increased. The cube-like shape indicates that the nanostructures are cuprous oxide (Cu_2O) rather than cupric oxide (CuO), where CuO usually exhibits sharp blade-like shapes [50]. Conversely, there were no noticeable morphology changes on both Ni thin films and coupons.

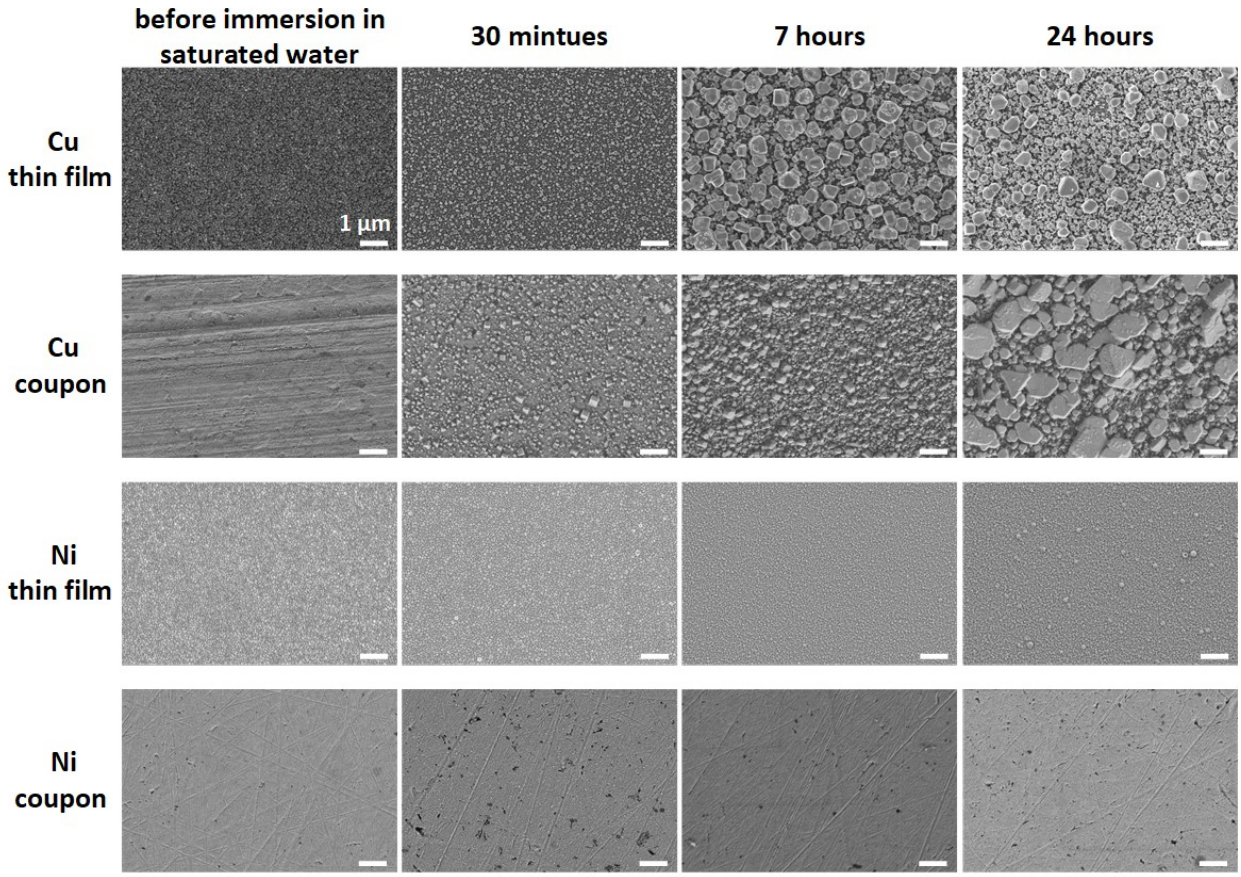

Figure 4. SEM images of Cu thin film, Cu coupon, Ni thin film, and Ni coupon surfaces before being immersed in saturated water and after boiling with different Δt. Cu shows growth in nanostructures as Δt increased, while changes in Ni surfaces were unnoticeable. All scale bars are 1 µm.

For detailed analysis of surface morphology, we measured surface profiles using AFM and characterized their root mean square roughness (R_{sq}) and surface area ratio (r) (Figure 5), where r is defined as the ratio of actual surface area to the projected area. We also characterized SiO_2 surfaces as a reference. The three-dimensional profile images of all samples appear in

Section III of the Supporting Information. The change in R_{sq} and r of Cu increased with Δt, similar to CHF. Specifically, Cu thin films showed significant increase in both R_{sq} and r, while Cu coupons showed a significant change in R_{sq} but the change in r remained less than 2.5%. This result implies that the shape of nanostructures on Cu thin films and coupons are different. A similar R_{sq} between thin films and coupons suggests the height of nanostructures was similar on both cases. The much higher r of thin films than coupons, on the other hand, indicates that the characteristic lateral size of nanostructures formed on thin films was smaller than coupons, so that the surface area increase on thin films was greater than that on coupons. This result was consistent with the SEM observation, where the 24 h Cu thin film showed relatively smaller lateral size of nanostructures than the nanostructures on the 24 h Cu coupon.

The morphology of Ni surfaces, as opposed to Cu, were stable for both thin films and coupons, which can explain the stable CHF values on Ni thin films. However, despite an observed change in CHF, the morphology of 24 h Ni coupon was not significantly changed as its CHF value. Although R_{sq} of 24 h Ni coupon increased slightly, the relative increase of CHF was more significant and comparable to that of Cu thin film sample, indicating that surface morphology is not the only important parameter governing CHF. The change in CHF as a function of R_{sq} and r area available in Section III of the Supporting Information.

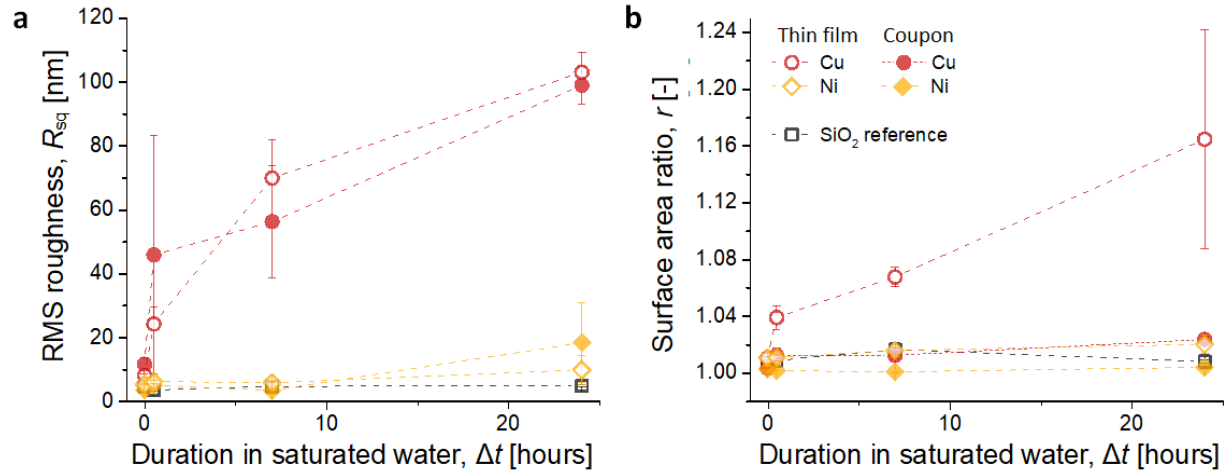

Figure 5. Statistical roughness parameters of Cu and Ni surfaces characterized by AFM. SiO_2 surfaces were characterized as a reference. Changes in root mean square roughness (a) and surface area ratio (b) as a function of Δt. Error bars represent standard deviations of measurements in three different spots. The three-dimensional profile images measured with AFM are available in Section IV of the Supporting Information.

3.3 Change in surface material composition

To observe the chemical oxidation states, we characterized surface material composition after boiling experiments using X-ray photoelectron spectroscopy (XPS) equipped with a monochromated Al Kα X-ray source (Versaprobe II XPS, Physical Electronics). The angle between the surface plane and the analyzer was 45°. All samples were sputtered with argon ions in the XPS chamber before the measurements to remove carbonaceous species from the surfaces. We collected principal Cu LMM Auger peaks on Cu thin films (Figure 6a) and coupons (Figure 6b) and plotted the normalized intensity as a function of kinetic energy (*KE*) of ejected Auger

electrons. Here the kinetic energy was converted from the electron binding energy (*BE*) and the energy of incident X-ray ($h\nu = 1486.6$ eV), i.e., $KE = h\nu - BE$. Both Cu thin films and coupons showed apparent shifts of Cu LMM peaks from Cu metal (~918.6 eV) to Cu_2O (~916.8 eV), indicating all Cu surfaces were oxidized in boiling water. In particular, the broad Cu LMM peak, spanning between Cu metal and Cu_2O peaks, of the 30 min Cu thin film represents the presence of CuO (~917.7 eV), which implies that the oxidation of Cu thin film surfaces transitions from CuO to Cu_2O as Δt increased.

The oxidation states of Ni thin films (Figure 6c) and Ni coupons (Figure 6d) were analyzed by the Ni2p spectra. While it was difficult to distinguish Ni2p multiplet-split peaks of Ni metal, Ni oxide (NiO), and Ni hydroxide ($Ni(OH)_2$), the clear appearance of NiO and $Ni(OH)_2$ satellite peaks on surfaces after boiling suggests that all Ni surfaces were oxidized in boiling water. Interestingly, the 24 h Ni coupon showed the presence of $Ni(OH)_2$ on the surface, whereas the other Ni surfaces showed the spectra of NiO only. This formation of $Ni(OH)_2$ could be originated from outgassed hydrogen from the Ni coupons. Bulk metals usually have dissolved hydrogens within their dislocation substructure [51], which can react with surface nickel to form $Ni(OH)_2$ when there is sufficient time for hydrogen to diffuse towards the surface. Considering that the 24 h Ni coupon also showed a notably higher CHF value than the other Ni surfaces, we attributed this result to be related to the material property of $Ni(OH)_2$. The primary material property that affects the CHF is known to be surface wettability. Specifically, the CHF model based on a receding contact angle has shown a reasonable agreement with experimental data [52]. To see the wettability difference between NiO and $Ni(OH)_2$, we measured advancing and receding contact angles by infusing and withdrawing water through a syringe, respectively, on 7

h and 24 h Ni coupon surfaces (Figure 6e and 6f). While both surfaces showed extremely small receding contact angles ($\lesssim 5°$), the advancing contact angle on the 24 h Ni coupon ($\approx 25°$) was smaller than that of the 7 h Ni coupon ($\approx 40°$), indicating that better wettability of $Ni(OH)_2$ compared with NiO could contribute to the increase in CHF observed on the 24 h Ni coupon. Alternatively, the outgassing hydrogen could also affect the measured CHF value by disrupting the nucleation behavior and bubble dynamics. Understanding this higher CHF value found on $Ni(OH)_2$ than NiO warrants further investigation in future work.

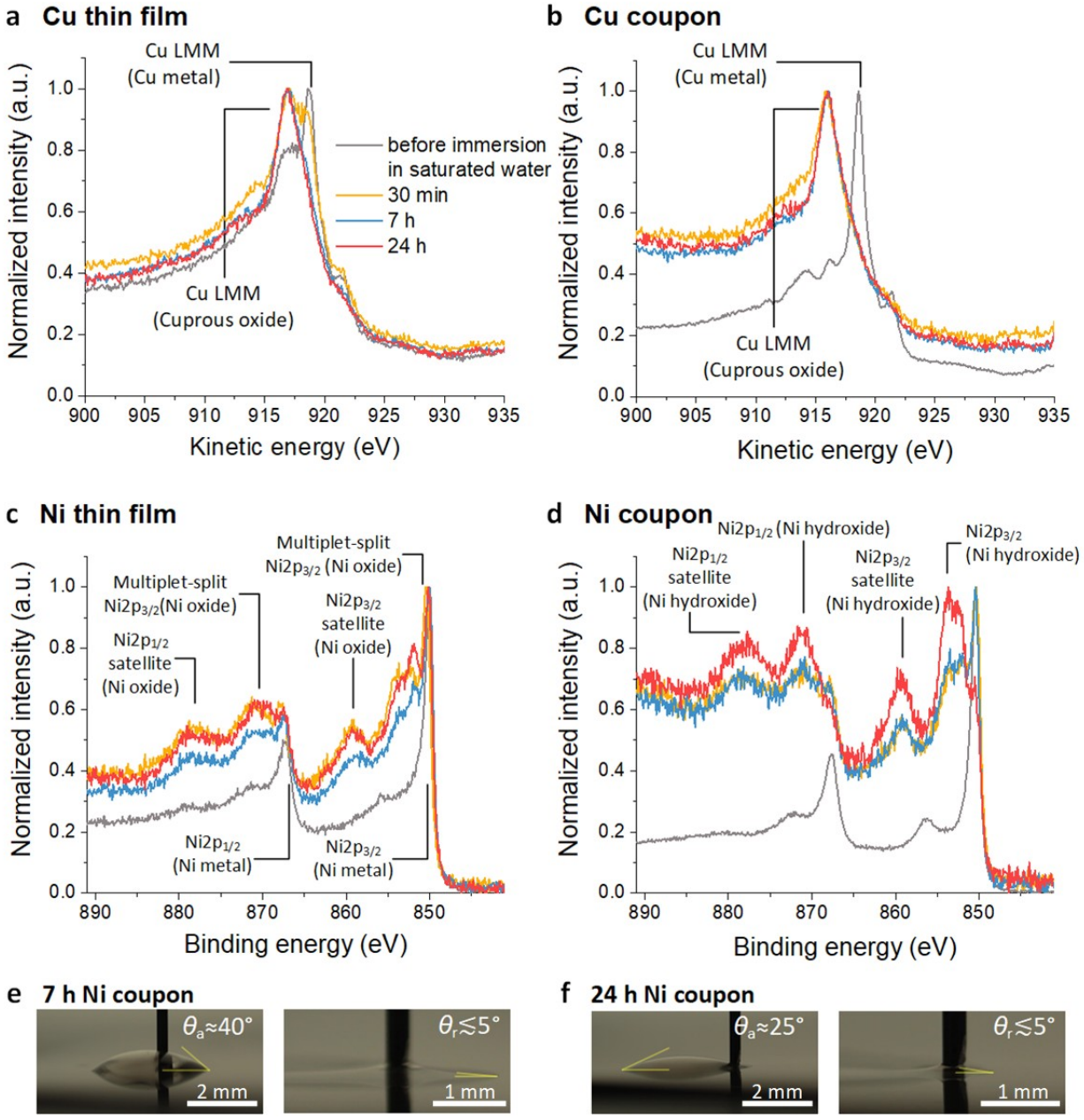

Figure 6. XPS analysis of Cu and Ni surfaces before being immersed in saturated water and after boiling. (a, b) Cu LMM Auger peaks on Cu thin films and coupons. All Cu surfaces showed evidence of Cu_2O. The surface composition of 30 min Cu thin film was under transition from CuO to Cu_2O. (c, d) Ni2p peaks on Ni thin films and coupons. All Ni surfaces showed evidence of oxidation. Particularly, the surface of 24 h Ni coupon was found to be $Ni(OH)_2$, while the

other Ni surfaces were NiO. (e, f) Advancing and receding contact angles of water on the 7 h and 24 h Ni coupon surfaces.

4. Conclusions

In this work, we addressed the discrepancy in reported CHF values of pool boiling of water on flat Cu and Ni surfaces by accounting for surface oxidation during boiling. We prepared 100 nm sputtered thin films and bulk metal coupons for Cu and Ni. Metallic surfaces were immersed in saturated water for different periods of time before pool boiling experiments. Along with pool boiling experiments, we analyzed the morphology of the surfaces using SEM and AFM and the chemical composition using XPS. The experimental results showed that pool boiling on metallic surfaces could be dependent on the samples' duration in saturated water. In the case of Cu surfaces, the roughness increased with residence time in saturated water by forming Cu_2O nanostructures, which led to an increase in CHF values due to the structural effects. The CHF and morphology of Ni surfaces were stable compared to Cu samples, with the exception of the 24 h Ni coupon, which exhibited a notably high CHF that could not be attributed to morphology. XPS analysis suggested the difference in CHF was likely due to a different surface chemical composition; the surface of the 24 h Ni coupon contained $Ni(OH)_2$, while the surfaces of the other Ni samples were primarily NiO. The reason why the $Ni(OH)_2$ surface exhibited a higher CHF than NiO surfaces could be attributed to its higher affinity for water, but this phenomenon requires further investigation. The measured CHF values of Cu (96.8 – 133.7 W/cm^2) and Ni (88.5 – 121.3 W/cm^2) fall within the spread of CHF values of Cu (60 – 157

W/cm^2) and Ni (78 – 168 W/cm^2) reported in the literature. The results of our study confirm that consistent control of samples' duration in saturated water is critical to achieve consistent measurements of pool boiling of water on metallic surfaces. In addition, we recommend that researchers characterize the morphology and chemical compositions of metallic surfaces before and after boiling to further investigate how changes in surface conditions affect the boiling heat transfer.

Authors' Contributions

Y. Song and D. J. Preston conceived the idea. Y. Song and H. Cha conducted pool boiling experiments. Y. Song, Z. Liu, and L. Zhang conducted the literature survey and XPS analysis. Y. Song and J. H. Seong prepared samples and analyzed morphology. Y. Song wrote the paper with input from all other authors. E. N. Wang guided the work.

Acknowledgements

Y. Song and H. Cha acknowledge that the information, data, or work presented herein was funded in part by the Advanced Research Projects Agency-Energy (ARPA-E), U. S. Department of Energy, under Award Number DE-AR0000ABC. L. Zhang acknowledges the Singapore-MIT Alliance for Research and Technology (SMART) program. Z. Liu and D. J. Preston acknowledge funding provided by the Rice University Faculty Initiatives Fund.

1

REFERENCES

[1] H.J. Cho, D.J. Preston, Y. Zhu, E.N. Wang, Nanoengineered materials for liquid–vapour phase-change heat transfer, Nat. Rev. Mater., 2 (2016) 16092, https://doi.org/10.1038/natrevmats.2016.92.

[2] N. Zuber, Hydrodynamic aspects of boiling heat transfer, Ph.D. Thesis, University of California, Los Angeles, Los Angeles, California, USA, 1959, doi:10.2172/4175511.

[3] Y. Song, L. Zhang, Z. Liu, D.J. Preston, E.N. Wang, Effects of airborne hydrocarbon adsorption on pool boiling heat transfer, Appl. Phys. Lett., 116(25) (2020) 253702, https://doi.org/10.1063/5.0012839.

[4] M.M. Rahman, E. Ölçeroğlu, M. McCarthy, Role of wickability on the critical heat flux of structured superhydrophilic surfaces, Langmuir, 30(37) (2014) 11225-11234, http://dx.doi.org/10.1021/la5030923.

[5] Y.-Y. Li, Z.-H. Liu, B.-C. Zheng, Experimental study on the saturated pool boiling heat transfer on nano-scale modification surface, Int. J. Heat Mass Transfer, 84 (2015) 550-561, https://www.sciencedirect.com/science/article/pii/S0017931014011727.

[6] E. Forrest, E. Williamson, J. Buongiorno, L.-W. Hu, M. Rubner, R. Cohen, Augmentation of nucleate boiling heat transfer and critical heat flux using nanoparticle thin-film coatings, Int. J. Heat Mass Transfer, 53(1) (2010) 58-67, https://www.sciencedirect.com/science/article/pii/S0017931009005481.

[7] Y.H. Maeng, S.L. Song, J.Y. Lee, Unaffectedness of improved wettability on critical heat flux enhancement with tio2 sputtered surface, Appl. Phys. Lett., 108(7) (2016) 074101, https://doi.org/10.1063/1.4942094.

[8] W. Bailey, E. Young, C. Beduz, Y. Yang, Pool boiling study on candidature of pentane, methanol and water for near room temperature cooling, in: Thermal and Thermomechanical Proceedings 10th Intersociety Conference on Phenomena in Electronics Systems, 2006. ITHERM 2006., 2006, pp. 599-603.

[9] H. Kim, H.S. Ahn, M.H. Kim, On the mechanism of pool boiling critical heat flux enhancement in nanofluids, J. Heat Transfer, 132(6) (2010), https://doi.org/10.1115/1.4000746.

[10] J.S. Coursey, J. Kim, Nanofluid boiling: The effect of surface wettability, Int. J. Heat Fluid Flow, 29(6) (2008) 1577-1585, https://www.sciencedirect.com/science/article/pii/S0142727X08001227.

[11] A.M. Gheitaghy, A. Samimi, H. Saffari, Surface structuring with inclined minichannels for pool boiling improvement, Appl. Therm. Eng., 126 (2017) 892-902, https://www.sciencedirect.com/science/article/pii/S1359431117312954.

[12] S. Mori, S. Mt Aznam, K. Okuyama, Enhancement of the critical heat flux in saturated pool boiling of water by nanoparticle-coating and a honeycomb porous plate, Int. J. Heat Mass Transfer, 80 (2015) 1-6, https://www.sciencedirect.com/science/article/pii/S0017931014007443.

[13] S.M. Kwark, G. Moreno, R. Kumar, H. Moon, S.M. You, Nanocoating characterization in pool boiling heat transfer of pure water, Int. J. Heat Mass Transfer, 53(21) (2010) 4579-4587, https://www.sciencedirect.com/science/article/pii/S0017931010003492.

[14] L. Liao, R. Bao, Z. Liu, Compositive effects of orientation and contact angle on critical heat flux in pool boiling of water, Heat Mass Transfer., 44(12) (2008) 1447-1453, https://doi.org/10.1007/s00231-008-0384-6.
[15] G. Chen, C.H. Li, Combined effects of liquid wicking and hydrodynamic instability on pool boiling critical heat flux by two-tier copper structures of nanowires and microgrooves, Int. J. Heat Mass Transfer, 129 (2019) 1222-1231, https://www.sciencedirect.com/science/article/pii/S0017931018325171.
[16] C.H. Li, R.P. Rioux, Independent and collective roles of surface structures at different length scales on pool boiling heat transfer, Sci. Rep., 6(1) (2016) 37044, https://doi.org/10.1038/srep37044.
[17] M.M. Rahman, J. Pollack, M. McCarthy, Increasing boiling heat transfer using low conductivity materials, Sci. Rep., 5 (2015) 13145, https://doi.org/10.1038/srep13145.
[18] W. Wu, H. Bostanci, L.C. Chow, Y. Hong, M. Su, J.P. Kizito, Nucleate boiling heat transfer enhancement for water and fc-72 on titanium oxide and silicon oxide surfaces, Int. J. Heat Mass Transfer, 53(9) (2010) 1773-1777, https://www.sciencedirect.com/science/article/pii/S0017931010000141.
[19] Y. Takata, S. Hidaka, M. Masuda, T. Ito, Pool boiling on a superhydrophilic surface, International Journal of Energy Research, 27(2) (2003) 111-119, https://onlinelibrary.wiley.com/doi/abs/10.1002/er.861.
[20] H. Auracher, W. Marquardt, Experimental studies of boiling mechanisms in all boiling regimes under steady-state and transient conditions, Int. J. Therm. Sci., 41(7) (2002) 586-598, https://www.sciencedirect.com/science/article/pii/S1290072902013522.
[21] C.H. Li, G. Peterson, Experimental study of enhanced nucleate boiling heat transfer on uniform and modulated porous structures, Frontiers in Heat and Mass Transfer, 1 (2010),
[22] C. Li, G.P. Peterson, Parametric study of pool boiling on horizontal highly conductive microporous coated surfaces, J. Heat Transfer, 129(11) (2007) 1465-1475, https://doi.org/10.1115/1.2759969.
[23] L. Bai, L. Zhang, G. Lin, G.P. Peterson, Pool boiling with high heat flux enabled by a porous artery structure, Appl. Phys. Lett., 108(23) (2016) 233901, https://aip.scitation.org/doi/abs/10.1063/1.4953574.
[24] Z. Yao, Y.W. Lu, S.G. Kandlikar, Effects of nanowire height on pool boiling performance of water on silicon chips, Int. J. Therm. Sci., 50(11) (2011) 2084-2090, http://www.sciencedirect.com/science/article/pii/S129007291100189X.
[25] M.M. Rahman, E. Ölçeroğlu, M. McCarthy, Scalable nanomanufacturing of virus-templated coatings for enhanced boiling, Adv. Mater. Interfaces, 1(2) (2014) 1300107, https://doi.org/10.1002/admi.201300107.
[26] S.H. Kim, G.C. Lee, J.Y. Kang, K. Moriyama, M.H. Kim, H.S. Park, Boiling heat transfer and critical heat flux evaluation of the pool boiling on micro structured surface, Int. J. Heat Mass Transfer, 91(Supplement C) (2015) 1140-1147, http://www.sciencedirect.com/science/article/pii/S0017931015008388.
[27] D.I. Shim, G. Choi, N. Lee, T. Kim, B.S. Kim, H.H. Cho, Enhancement of pool boiling heat transfer using aligned silicon nanowire arrays, ACS Appl. Mater. Interfaces, 9(20) (2017) 17595-17602, http://dx.doi.org/10.1021/acsami.7b01929.
[28] A. Zou, S.C. Maroo, Critical height of micro/nano structures for pool boiling heat transfer enhancement, Appl. Phys. Lett., 103(22) (2013) 221602, https://doi.org/10.1063/1.4833543.

[29] B.S. Kim, H. Lee, S. Shin, G. Choi, H.H. Cho, Interfacial wicking dynamics and its impact on critical heat flux of boiling heat transfer, Appl. Phys. Lett., 105(19) (2014) 191601, https://doi.org/10.1063/1.4901569.
[30] R. Chen, M.-C. Lu, V. Srinivasan, Z. Wang, H.H. Cho, A. Majumdar, Nanowires for enhanced boiling heat transfer, Nano Lett., 9(2) (2009) 548-553, https://doi.org/10.1021/nl8026857.
[31] N.S. Dhillon, J. Buongiorno, K.K. Varanasi, Critical heat flux maxima during boiling crisis on textured surfaces, Nat. Commun., 6 (2015) 8247, http://dx.doi.org/10.1038/ncomms9247.
[32] A.R. Betz, J. Jenkins, C.-J.C. Kim, D. Attinger, Boiling heat transfer on superhydrophilic, superhydrophobic, and superbiphilic surfaces, Int. J. Heat Mass Transfer, 57(2) (2013) 733-741, http://www.sciencedirect.com/science/article/pii/S0017931012008460.
[33] A.R. Betz, J. Xu, H. Qiu, D. Attinger, Do surfaces with mixed hydrophilic and hydrophobic areas enhance pool boiling?, Appl. Phys. Lett., 97(14) (2010) 141909, https://doi.org/10.1063/1.3485057.
[34] H.S. Ahn, J.M. Kim, M. Kaviany, M.H. Kim, Pool boiling experiments in reduced graphene oxide colloids. Part i – boiling characteristics, Int. J. Heat Mass Transfer, 74 (2014) 501-512, http://www.sciencedirect.com/science/article/pii/S0017931014000507.
[35] K.-H. Chu, R. Enright, E.N. Wang, Structured surfaces for enhanced pool boiling heat transfer, Appl. Phys. Lett., 100(24) (2012) 241603, https://doi.org/10.1063/1.4724190.
[36] A. Zou, D.P. Singh, S.C. Maroo, Early evaporation of microlayer for boiling heat transfer enhancement, Langmuir, 32(42) (2016) 10808-10814, https://doi.org/10.1021/acs.langmuir.6b02642.
[37] H. Jo, S. Kim, H.S. Park, M.H. Kim, Critical heat flux and nucleate boiling on several heterogeneous wetting surfaces: Controlled hydrophobic patterns on a hydrophilic substrate, Int. J. Multiphase Flow, 62 (2014) 101-109, http://www.sciencedirect.com/science/article/pii/S030193221400041X.
[38] H.S. Ahn, J.M. Kim, C. Park, J.-W. Jang, J.S. Lee, H. Kim, M. Kaviany, M.H. Kim, A novel role of three dimensional graphene foam to prevent heater failure during boiling, Sci. Rep., 3 (2013) 1960, https://doi.org/10.1038/srep01960.
[39] H. Seo, Y. Lim, H. Shin, I.C. Bang, Effects of hole patterns on surface temperature distributions in pool boiling, Int. J. Heat Mass Transfer, 120 (2018) 587-596, http://www.sciencedirect.com/science/article/pii/S0017931017340528.
[40] H. Jo, D.I. Yu, H. Noh, H.S. Park, M.H. Kim, Boiling on spatially controlled heterogeneous surfaces: Wettability patterns on microstructures, Appl. Phys. Lett., 106(18) (2015) 181602, https://doi.org/10.1063/1.4919916.
[41] H. O'Hanley, C. Coyle, J. Buongiorno, T. McKrell, L.-W. Hu, M. Rubner, R. Cohen, Separate effects of surface roughness, wettability, and porosity on the boiling critical heat flux, Appl. Phys. Lett., 103(2) (2013) 024102, https://doi.org/10.1063/1.4813450.
[42] D.E. Kim, S.C. Park, D.I. Yu, M.H. Kim, H.S. Ahn, Enhanced critical heat flux by capillary driven liquid flow on the well-designed surface, Appl. Phys. Lett., 107(2) (2015) 023903, https://doi.org/10.1063/1.4926971.
[43] M. Može, M. Zupančič, I. Golobič, Investigation of the scatter in reported pool boiling chf measurements including analysis of heat flux and measurement uncertainty evaluation methodology, Appl. Therm. Eng., 169 (2020) 114938, https://www.sciencedirect.com/science/article/pii/S1359431119359459.

[44] J.H. Lienhard, V.K. Dhir, D.M. Riherd, Peak pool boiling heat-flux measurements on finite horizontal flat plates, J. Heat Transfer, 95(4) (1973) 477-482, https://doi.org/10.1115/1.3450092.
[45] Z. She, V.K. Dhir, Parametric effects of heater size, contact angle, and surrounding vessel size on pool boiling critical heat flux from horizontal surfaces, Journal of Electronic Packaging, (2021), https://doi.org/10.1115/1.4052716.
[46] I.I. Gogonin, S.S. Kutateladze, Critical heat flux as a function of heater size for a liquid boiling in a large enclosure, Journal of engineering physics, 33(5) (1977) 1286-1289, https://doi.org/10.1007/BF00860899.
[47] A. Hedin, A.J. Johansson, C. Lilja, M. Boman, P. Berastegui, R. Berger, M. Ottosson, Corrosion of copper in pure o2-free water?, Corros. Sci., 137 (2018) 1-12, https://www.sciencedirect.com/science/article/pii/S0010938X17306534.
[48] N.S. Saadi, L.B. Hassan, T. Karabacak, Metal oxide nanostructures by a simple hot water treatment, Sci. Rep., 7(1) (2017) 7158, https://doi.org/10.1038/s41598-017-07783-8.
[49] P.L. Andresen, J. Hickling, A. Ahluwalia, J. Wilson, Effects of hydrogen on stress corrosion crack growth rate of nickel alloys in high-temperature water, Corrosion, 64(9) (2008) 707-720, https://doi.org/10.5006/1.3278508.
[50] K.R. Khedir, Z.S. Saifaldeen, T.M. Demirkan, A.A. Al-Hilo, M.P. Brozak, T. Karabacak, Robust superamphiphobic nanoscale copper sheet surfaces produced by a simple and environmentally friendly technique, Adv. Eng. Mater., 17(7) (2015) 982-989, https://onlinelibrary.wiley.com/doi/abs/10.1002/adem.201400397.
[51] M.R. Louthan, J.A. Donovan, G.R. Caskey, Hydrogen diffusion and trapping in nickel, Acta Metall., 23(6) (1975) 745-749, https://www.sciencedirect.com/science/article/pii/0001616075900577.
[52] S.G. Kandlikar, A theoretical model to predict pool boiling chf incorporating effects of contact angle and orientation, J. Heat Transfer, 123(6) (2001) 1071-1079, https://doi.org/10.1115/1.1409265.